

DNA Ternary Full Adder

Enqiang Zhu¹, Peize Qiu¹, Xianhang Luo² ✉, Chanjuan Liu³ ✉, and Jin Xu⁴

¹Institute of Computing Science and Technology, Guangzhou University, Guangzhou 510006, China

²School of Computer Science and Technology, Wuhan University of Science and Technology, Wuhan 430065, China

³School of Computer Science and Technology, Dalian University of Technology, Dalian 116024, China

⁴School of Computing Science, Peking University, Beijing 100871, China

✉ Corresponding authors: 202313601008@wust.edu.cn; chanjuanliu@dlut.edu.cn

ABSTRACT

As transistor dimensions continue to shrink, binary devices are rapidly approaching their fundamental limits in power density. In response, multi-valued systems have attracted significant attention due to their enhanced information density. Among these, the ternary system stands out as the most practical option, being the closest integer base to e , which is considered optimal for information efficiency. Despite the intrinsic advantages of DNA nanomaterials, such as programmability, energy efficiency, and massive parallelism, their application in ternary logic remains largely unexplored, particularly in the realm of ternary addition circuits. This gap can be attributed to a fundamental challenge: ternary logic requires circuits capable of recognizing and processing a far larger set of input combinations than binary systems, a task that existing models and techniques often struggle to accomplish. In this work, we propose a novel architecture for a ternary full adder. Our design includes a competitive blocking (CB) circuit that enables the recognition and computation of all possible three-input ternary combinations. Coupled with a dynamic concentration adjustment (CA) strategy, this approach significantly enhances the number of trits that can be processed. Biochemical experiments demonstrate that the CB circuit successfully yields the correct output digits for a ternary full adder, achieving 17-trit ternary addition. To our knowledge, this work represents the first successful DNA-based ternary adder, establishing a new methodological foundation for DNA computing and highlighting its considerable potential for scalable digital information processing.

Keywords: DNA ternary adder; competitive blocking circuit; concentration adjustment.

Introduction

Molecular systems represent a revolutionary intersection of biology, computing, and engineering, offering unique capabilities that traditional silicon-based systems cannot match¹. By leveraging the Watson-Crick base-pairing principle, DNA molecules exhibit remarkable programmability at the molecular level, enabling them to evolve into a novel computational paradigm. Since Adleman² first employed DNA to solve the traveling salesman problem, DNA computing has attracted significant attention. DNA molecules are no longer seen merely as a carrier of genetic information; it is increasingly utilized as a sophisticated engineering material across various research fields³, including the development of DNA nanostructures⁴⁻⁶, the construction of DNA logic gates⁷⁻⁹, and applications in disease detection¹⁰⁻¹³. DNA computing offers remarkable advantages in parallel processing, which greatly enhances computational efficiency^{14,15}.

The toehold-mediated strand displacement (TMSD) plays a crucial role in DNA computing due to its unique properties. Firstly, it operates spontaneously and stably at room temperature without requiring enzymes^{16,17}. Secondly, TMSD demonstrates precise sequence orthogonality, enabling specific interactions among different sequences. This characteristic is essential for constructing complex computational networks, thereby significantly enhancing computational accuracy and reliability^{18,19}. By leveraging TMSD technology, researchers have successfully created a range of molecular computing devices²⁰⁻²⁷. Among them, the “seesaw” gates introduced by Qian and Winfree were the first to realize large-scale digital circuits²⁸ and neural networks²⁹, and are now regarded as the cornerstone of scalable strand-displacement logic. Meanwhile, DNA tile-based computing³⁰⁻³² and TMSD circuits on top of DNA origami³³⁻³⁶ have further spatialized and structured computational units, expanding the design dimensions. In addition, some studies have focused on optimizing the TMSD reaction process, including suppressing leakage³⁷, enhancing signal output^{38,39}, and tuning reaction kinetics⁴⁰. These advances provide important theoretical support for the field of DNA computing.

Among the various molecular computing devices, the prominence of addition operations is particularly pronounced. Addition serves as the cornerstone of a myriad of digital arithmetic operations, including magnitude comparison⁴¹, multiplication^{42,43}, and subtraction⁴⁴. Furthermore, it constitutes a core component of arithmetic modules within digital microprocessors⁴⁵, where its performance directly dictates the overall efficiency of the computing system. Consequently, DNA adders, which exemplify

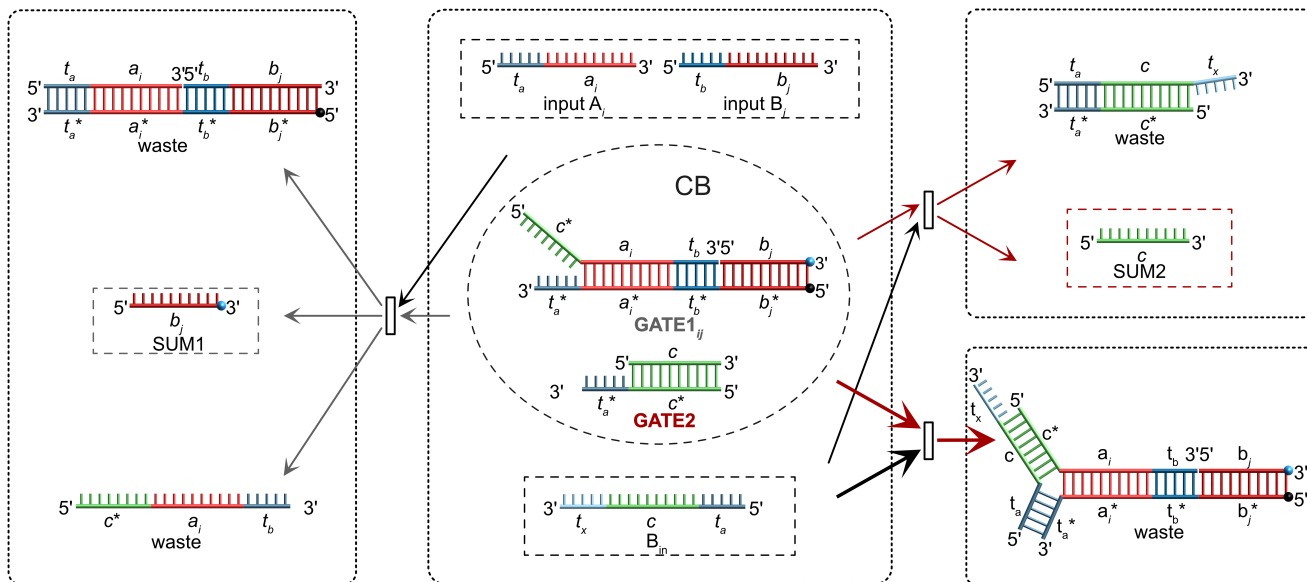


Figure 1. The illustration depicts the operational mechanism of the CB circuit, which encompasses three core reactions corresponding to Equations 1, 2, and 3. All reactions involving $GATE1_{ij}$ are represented by gray arrows, while those involving $GATE2$ are indicated with red arrows. It is particularly noteworthy that the reaction efficiency between $GATE1_{ij}$ and B_{in} is the highest. To emphasize this significant difference in efficiency, we have intentionally employed a thicker red arrow to represent the reaction between $GATE2$ and B_{in} .

the construction of fundamental arithmetic operations from DNA logic gates, demonstrate TMSD's profound potential for implementing intricate logical functions at the molecular level, thereby establishing a foundation for DNA computing models for more sophisticated tasks⁴⁶.

Considerable efforts have been devoted to building DNA adders. Early logic gates primarily utilized binary encoding, employing single-stranded DNA as input and optical or electrical signals as output^{47,48}. These pioneering efforts successfully constructed fundamental logic gates, including XOR and AND gates⁴⁹. Then, Li et al.⁵⁰ combined these XOR and AND gates to develop a half-adder. However, its complex logic-gate design, which exhibits low integration efficiency, makes the DNA full adder difficult to implement. For this, Su et al.⁵¹ applied dual-rail DNA logic gates by paralleling single-rail AND and OR gates, effectively integrating a 1-bit full adder with a 4:1 multiplexer to realize a vital DNA arithmetic logic unit. To further simplify circuit complexity, Wang et al.²⁵ proposed a strategy based on the principle that "any digital circuit can be represented by a set of equations, with equation terms corresponding to specific switches in the circuit." This approach employed TMSD to create DNA switch circuits for molecular digital computing, using only 20% of the DNA strands compared with dual-rail logic expressions. In addition, some studies have achieved DNA adders by introducing complex structures, such as DNA tetraplexes⁵² and DNA origami⁴⁶. However, many molecular designs within these structures face scalability issues that impede effective signal transmission. Although Tandon et al.⁵³ designed a DNA tile-based calculator capable of performing addition on 6-bit binary numbers, its experimental operation and system design are more complex. To overcome these challenges, Xie et al.⁵⁴ designed a scalable DNA full adder based on cooperative strand-displacement reactions. By developing a dual logic gate capable of simultaneously performing XOR and AND operations, they significantly reduced the number of DNA strands required for the computation. Furthermore, Stérin et al.⁵⁵ implemented the addition of up to 25 bits by combining thermodynamics and self-assembly techniques.

However, existing DNA adders are all based on binary encoding. From the perspective of information economy, the e-ary system is superior (see Supporting Information, Section S3). Specifically, when representing numbers over the same range, the product of base and width for the e-ary system is smaller than that for binary, meaning that under ideal conditions the e-ary system can achieve the same computational scale with fewer resources⁵⁶. The e-ary system is closest to the ternary system. Moreover, studies have shown that when binary Boltzmann transistors in traditional CMOS technology approach the power density limit, the most effective way to significantly increase information density (N) is to switch from a binary system to a ternary system, where the system complexity is reduced to $C = \log_3 N / \log_2 N \approx 63.1\%$ ⁵⁷. Unfortunately, ternary logic faces an inherent challenge: by its nature, it requires the circuit to recognize and correctly compute a far greater number of input combinations than binary systems, a requirement that cannot be met with existing models or techniques. Consequently, a ternary adder has not yet been experimentally realized in DNA computing.

To fill this gap, this paper proposes a DNA-based ternary adder architecture. Full adders require flexible handling of carry information, a challenge necessitating precise chemical reaction network design. To address this, our study designed a competitive blocking (CB) circuit to accurately recognize and manage the carry information from prior calculations along with the two current addend information (i.e., a total of three inputs, giving 18 possible combinations). The core of this circuit lies in its clever utilization of differences in reaction rate constants (e.g., $k_2 \gg k_1, k_3$ in reactions 1, 2, 3) to enable dynamic selection and blocking of reaction pathways, essentially functioning as a logic control based on chemical kinetics. Biochemical experiments demonstrate that the CB circuit can reliably determine whether a carry occurred in prior computations and rapidly respond by selecting the corresponding reaction path. Furthermore, this research, for the first time, successfully integrated ternary logic with the proposed concentration adjustment (CA) strategy and, based on the CB circuit, designed and implemented a DNA ternary full adder. The CA strategy aims to minimize the demand for carry information during computation, thereby significantly enhancing the computational capacity of multi-digit adders. It essentially applies the principle of chemical equilibrium, using a "divide and conquer" approach to enable the circuit to regulate reactant concentration ratios, thus optimizing signal transmission efficiency. Compared with existing technologies, this study has achieved several major breakthroughs. Specifically, we have achieved 17 consecutive carries in ternary form, which, to the best of our knowledge, represents the highest computational scale reported to date for DNA adders. Moreover, compared with several state-of-the-art DNA adders, our adder performs favorably across various evaluation metrics (e.g., scale per strand, strands per digit; see Supporting Information, Section S1 for detailed comparisons). Furthermore, biochemical experimental results confirm that our proposed CA strategy makes our DNA multi-digit ternary adder easily adaptable to calculations involving even higher digit counts. More importantly, the successful application of this new strategy, based on molecular competitive dynamics (k -control) and reactant concentration regulation (chemical equilibrium), provides novel insights and tools for designing and constructing more complex and robust chemical reaction-based molecular systems.

Results

The Competitive Blocking Circuit. The principle of the CB circuit is illustrated in Figure 1. It consists of two logic gates, denoted GATE1_{ij} and GATE2, representing two levels of reaction. The CB circuit has two input signals, denoted as inputA_i and inputB_j, along with a blocking signal B_{in}. The signal B_{in} can be in a logic state of either *present* or *absent*, indicating whether it participates in the reaction. Here, $i, j \in \{0, 1, 2\}$ represent the ternary numbers involved in the addition operation. When B_{in} is in the *absent* state, the CB circuit receives inputA_i and inputB_j as inputs, activating the first level of reaction. This means that the two inputs interact with GATE1_{ij} to produce an output signal, denoted as SUM1. Conversely, when B_{in} is *present*, it reacts with GATE1_{ij}, effectively consuming GATE1_{ij} and thereby inhibiting the first level of reaction between GATE1_{ij} and the inputs inputA_i and inputB_j. Furthermore, the presence of B_{in} can activate the second level of the reaction, leading to a reaction with GATE2 and producing a different output signal, denoted as SUM2.

The CB mechanism can be expressed via the following reactions:



Specifically, GATE1_{ij} is a stable structure formed through base pairing in the a_i , t_b , and b_j domains, while the toehold sites t_a^* and c^* remain exposed. The inputA_i strand contains the toehold t_a and the long domain a_i . The toehold t_a of inputA_i initiates a TMSD by pairing with the t_a^* site on GATE1_{ij} and continues base pairing until the strand incorporating c^* , a_i , and t_b is displaced (The short domain t_b will break free because the two longer domains c^* and a_i are in a free state). As a result, the t_b^* site becomes exposed. Since inputB_j contains the toehold t_b and the long domain b_j , it undergoes a similar TMSD by pairing with the t_b^* site, thus displacing the fluorescently labeled single strand b_j . This indicates the generation of SUM1. This process is described by Equation 1 and illustrated in Figure 1.

The blocking strand B_{in} contains the toehold t_a along with the long domains c and t_x . The toehold t_a binds to the t_a^* site of GATE1_{ij}, effectively locking it through the complementary base pairing principle of DNA (Equation 2 and Figure 1). Given that the toehold t_a comprises only five bases, there is a risk of detachment after locking solely by this interaction. To mitigate this risk, we have added domain c^* to the 5' end of domain a_i to enhance the stability of B_{in}'s binding to GATE1_{ij}, ensuring that the toehold t_a^* remains firmly locked. We conducted an evaluation of the binding stability of B_{in} to GATE1_{ij} both before and subsequent to the addition of domain c^* . The results indicate that GATE1_{ij} exhibits a higher binding efficacy with B_{in} following the incorporation of domain c^* (see Supporting Information S4). This design effectively prevents the toehold t_a in inputA_i from

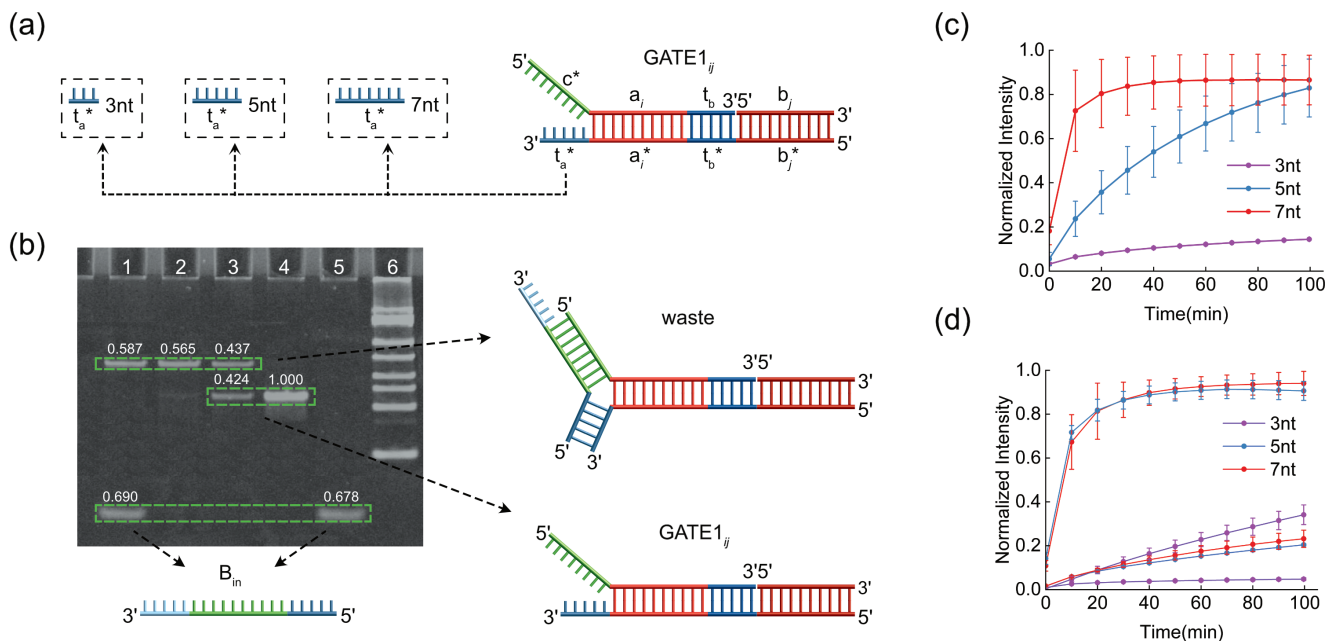


Figure 2. (a) Test schemes for different toehold lengths in the $GATE1_{ij}$ structure. (b) Polyacrylamide gel electrophoresis (PAGE) results show binding between B_{in} and $GATE1_{ij}$ in the CB circuit at different concentration ratios, where the relative concentration of each band is determined by its brightness. (c) Fluorescence detection results for SUM1 product generated by the CB circuit when the toehold lengths of $GATE1_{ij}$ are 3nt, 5nt, and 7nt, respectively. (d) Fluorescence results for SUM2 product generated by the CB circuit when the toehold lengths of $GATE1_{ij}$ are 3nt, 5nt, and 7nt. Solid lines in this figure represent the fluorescence signal of SUM2, while dashed lines indicate the leakage of SUM1 due to B_{in} not fully locking $GATE1_{ij}$.

engaging in a TMSD with the t_a^* site of the gate structure, thereby ensuring that the output strand modified with fluorescence is not displaced. Upon locking $GATE1_{ij}$, the reaction proceeds with $GATE2$. $GATE2$ is a stable structure formed through base pairing in the c domain, while the toehold site t_a^* remains exposed. The blocking strand B_{in} engages in a TMSD with the exposed toehold site t_a^* of $GATE2$ (Equation 3 and Figure 1), leading to the displacement of the output strand that carries the fluorescence modification. The resulting computational output, SUM2, can be determined by analyzing the fluorescent signal.

The length of the toehold is pivotal in determining the rate of the TMSD^{40,58}. We evaluated the effect of three common toehold lengths of 3nt, 5nt, and 7nt on our reaction rates (Figure 2a). The fluorescence data (Figure 2c) indicate that with a 3nt toehold, the increase in fluorescence intensity is minimal, reflecting a low reaction efficiency. In contrast, extending the toehold length to 5nt and 7nt markedly accelerates the reaction rate, achieving a peak within 30 minutes. Therefore, we excluded the 3nt toehold from further consideration. Additionally, the binding efficiency of B_{in} to $GATE1_{ij}$ affects the accuracy of the first-level reaction, as a portion of it still occurs even when B_{in} is present. We call this a leakage reaction. To address this, we examined SUM1 leakage across different toehold lengths. The experimental findings are illustrated in Figure 2d. On the one hand, when using a 3nt toehold, the fluorescence of the leakage reaction producing SUM1 is minimal; however, SUM2 formation is too slow. On the other hand, although the reaction with a 7nt toehold is faster than that with a 5nt toehold, it results in greater leakage of the incorrect result SUM1. Consequently, we opted for a 5nt toehold length to minimize the generation of leakage reaction.

Based on the experimental results for a toehold length of 5 nucleotides, as presented in Figure 2c and Figure 2d, the rates of critical reactions within the CB circuit are detailed as follows. The rate k_1 of Reaction 1 (Equation1, which is where input A_i and input B_j interact with $GATE1_{ij}$) is measured at $1.1876 \times 10^{-4} \mu\text{M/s}$. In comparison, the rate k_2 of Reaction 2 (Equation2, which is where B_{in} binds to $GATE1_{ij}$) is significantly higher at $1.8377 \times 10^{-3} \mu\text{M/s}$, while the rate k_3 of Reaction 3 (Equation3, which is where B_{in} interacts with $GATE2$) stands at $7.2992 \times 10^{-4} \mu\text{M/s}$. Further details on the calculation of these rates are provided in Supporting Information S1.3. These results clearly indicate that the reaction rate of Reaction 2 is substantially greater than that of Reaction 1 and 3. This suggests that in the presence of B_{in} , it will preferentially and rapidly bind to $GATE1_{ij}$, effectively inhibiting Reaction 1. Following this, B_{in} proceeds to react with $GATE2$. Conversely, when B_{in} is absent, the CB circuit will proceed with Reaction 1. Additionally, to verify whether the B_{in} successfully locks the gate, we examined the binding between B_{in} and $GATE1_{ij}$ at varying B_{in} concentrations. Polyacrylamide gel electrophoresis (PAGE) was performed; the results are shown in Fig. 2b. From left to right, the molar ratios of B_{in} to $GATE1_{ij}$ are 1.5:1, 1:1, 0.5:1, 0:1, and 1:0.

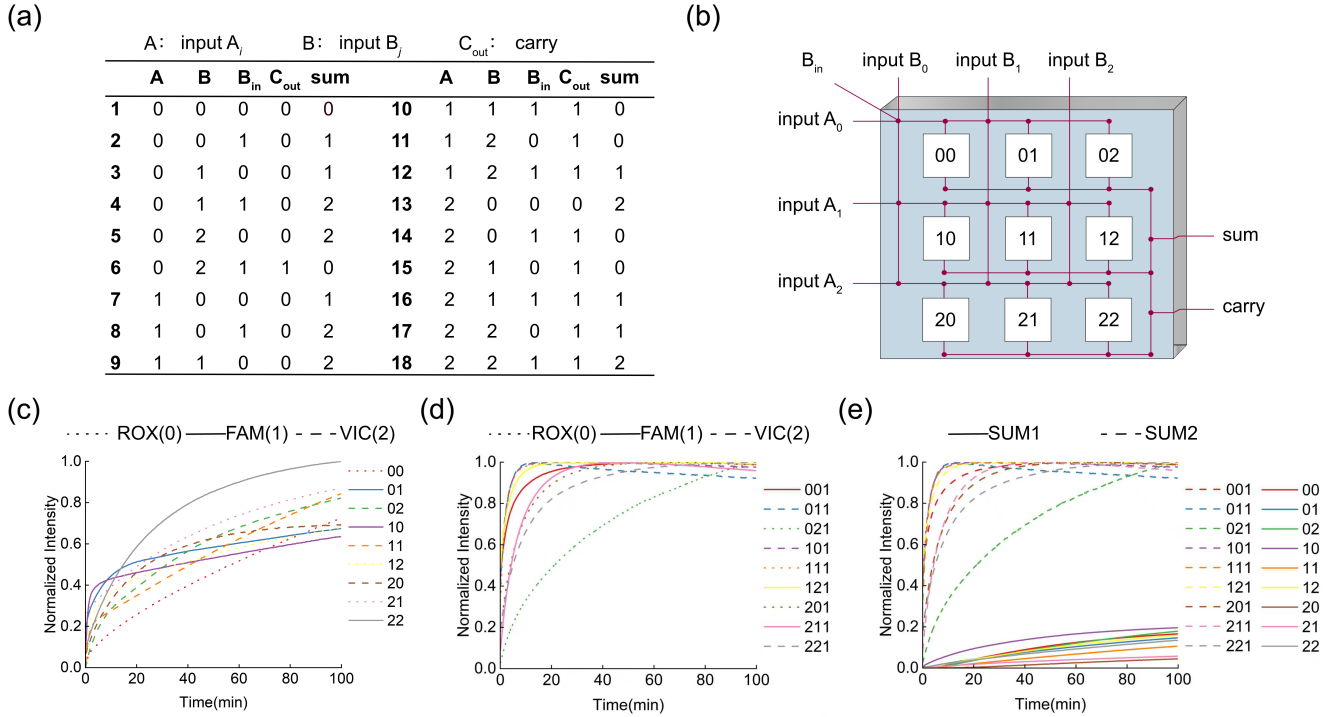


Figure 3. (a) Truth table for the ternary adder. (b) Modular processing of the ternary adder based on its truth table. (c) Fluorescence curves for all reactions of the half adder. The results were normalized to the maximum fluorescence across all samples, and a fluorescence reading above 0.5 was considered a valid output. (d) Fluorescence curves for the SUM2 result in the 1-trit full adder. The current results were normalized to their respective maximum fluorescence values, and the output reflects the fluorescence type with the highest fluorescence. (e) Fluorescence curves for all reactions of the 1-trit full adder. All fluorescence types in the current results were normalized to their respective maximum fluorescence values; solid lines represent SUM2. Dashed lines denote SUM1 leakage, attributed to the carry information from the preceding digit not completely locking the $GATE1_{ij}$.

Evidently, when B_{in} is present, it binds efficiently to $GATE1_{ij}$. In lane 3, a fraction of $GATE1_{ij}$ remains unbound because the B_{in} concentration is lower than that of $GATE1_{ij}$. When the B_{in} concentration is equal to or higher than that of $GATE1_{ij}$ (lanes 1 and 2), all $GATE1_{ij}$ molecules are bound by B_{in} . We therefore conclude that B_{in} can effectively bind to $GATE1_{ij}$.

Moreover, we experimentally demonstrated the robustness of the CB circuit to sequence design choices and its tolerance to noise. First, we tested the stability of the CB circuit under different sequences. A total of nine distinct scenarios were examined, corresponding to the nine input- B_{in} combinations of the ternary full adder (Figure S19). Subsequently, we tested the effect of B_{in} on the CB circuit under varying GC content conditions (see Section S5 of the Supporting Information). The results indicate that the CB circuit consistently produces correct outputs across these varied sequences. Second, we evaluated the circuit's stability in the presence of noise, including mismatches and unrelated strands (see Section S5 of the Supporting Information). The findings confirm that the CB circuit remains functional and yields accurate results even under noisy conditions.

A Ternary DNA Full Adder Design Using CB Circuit. The design of the ternary full adder, based on the CB circuit, comprises four key components: converting input digits into DNA strands, computing the sum and carry, translating output signals into results, and extracting carry information as input to the next digit. Each digit's input and output in a ternary adder can take three possible values (0, 1, or 2). This makes the conventional dual-rail strategy difficult to apply⁵¹. To address this, we employed a triple-rail method to represent the three input and output states. Specifically, we designate input A_0 , input A_1 , and input A_2 to convey the inputs for 0, 1, and 2, while utilizing input B_0 , input B_1 , and input B_2 for similar representations. Each input A_i consists of a toehold t_a and domain a_i , and each input B_j comprises a toehold t_b and domain b_j , where $i, j \in \{0, 1, 2\}$. Additionally, we employ three distinct fluorescent signals (ROX, FAM, VIC) to visualize the resulting outputs corresponding to 0, 1, and 2. It's worth noting that the fluorescent signal types assigned to each module's Gate2 and $GATE1_{ij}$ follow a specific pattern, as detailed in Table 4 of Section S15 in the Supporting Information.

Compared to traditional binary adders, the number of input combinations involved in this computation process differs significantly. The input combinations for a traditional binary adder amount to $2^3 = 8$ possibilities, as its inputs are limited to two states: 0 and 1. This simplicity enables straightforward implementation using conventional circuits. In contrast, the

ternary adder presents a much more complex scenario; it features up to $2 \times 3^2 = 18$ input combinations (see Figure 3a), which poses significant challenges for implementation using standard circuits. To address this complexity, we modularize the design into nine distinct modules, termed ij -modules (where $i, j \in \{0, 1, 2\}$), inspired by the principles of computer memory addressing. Based on the CB circuit, these ij -modules are capable of computing $i + j + x$ (where x is 0 or 1, representing the presence or absence of carry information), thereby generating the result information SUM1 or SUM2 (Figure 3b and Supporting Information, Figure S8 - S16).

According to the truth table (Figure 3a), there are nine scenarios that result in carry information. We categorize these scenarios into two types for processing.

The first type involves carry generation through a three-input AND gate. This includes cases 6, 10, and 14, where a carry is generated only in the presence of B_{in} (the carry input from the previous digit). This indicates that the production of carry information relies on the inputs $inputA_i$, $inputB_j$, and B_{in} . Consequently, we implement this function using a three-input AND gate ($GATE1_{ij}^-$, where $ij \in \{02, 11, 20\}$), as illustrated in Figure 4a). The structure of $GATE1_{ij}^-$ comprises four single strands, which stabilize through base pairing in the toehold regions t_a and t_b , along with the longer domains a_i , b_j , and c . At the same time, it reveals the toehold site t_a^* and the longer domain r . When all three inputs, $inputA_i$, $inputB_j$, and B_{in} , are present, this gate produces the carry information strand cr . The specific reaction mechanism is depicted in Figure 4a. Initially, the toehold t_a of $inputA_i$ binds to the exposed toehold t_a^* of $GATE1_{ij}^-$. This interaction facilitates the engagement of the long domain a_i of $inputA_i$ with the domain a_i^* within $GATE1_{ij}^-$, leading to the release of domain a_i from $GATE1_{ij}^-$. As t_a consists of only five bases, the strand $a_i t_b$ will subsequently detach once domain a_i is liberated, thereby exposing the toehold t_b^* . Subsequently, a parallel reaction will displace the strand $b_j t_a$ upon the introduction of $inputB_j$, which in turn reveals the toehold t_a^* . At this juncture, if the carry information B_{in} from the previous digit is present, it will bind to the exposed toehold t_a^* and displace the information strand cr through a TMSD.

The second type involves carry generation through a two-input AND gate in conjunction with a conversion gate. This category includes cases 11, 12, 15, 16, 17, and 18. In these scenarios, a carry is generated for the subsequent digit regardless of the carry input B_{in} . This indicates that the carry information relies exclusively on $inputA_i$ and $inputB_j$. We implement this function using a two-input AND gate $GATE_{ij}^-$, where $ij \in \{12, 21, 22\}$ (see Figure 4b)). The structure of $GATE_{ij}^-$ consists of three single strands stabilized through base pairing at the toehold t_b , along with the longer domains a_i and b_j . It also features the toehold site t_a^* and a longer domain r . When both $inputA_i$ and $inputB_j$ are present, this gate produces an output. The specific reaction mechanism is illustrated in Figure 4b. Similar to the first type, when $inputA_i$ and $inputB_j$ are both present, the strands $a_i t_b$ and $b_j r$ are sequentially displaced. It is important to highlight that this reaction does not directly yield the carry information strand cr ; instead, it produces an intermediate strand $b_j r$. To resolve this issue, we devised a conversion gate $GATE\text{-Convert}b_j$ for $j = 1, 2$ (as shown in Figure 4b). The structure of $GATE\text{-Convert}b_j$ consists of two single strands, one of which contains the necessary carry information. These strands are stabilized through base pairing involving their domain r . Furthermore, the gate includes a toehold site b_j^* and a domain c . When the intermediate strand $b_j r$ is available, this gate will produce an output, effectively transforming $b_j r$ into the carry information strand cr for subsequent extraction processes.

To extract the carry information and transfer it to the subsequent digit calculation, we designed an extractor referred to as $GATE\text{-Extract}$ (Figure 4c). This structure forms a hairpin shape through self-complementary base pairing between the domains c and c^* , with the toehold t_r embedded within the hairpin. As shown in Figure 4c, when the carry information is present in the test tube, the domain r^* of the hairpin engages in a TMSD with the domain r of the information strand cr . This reaction opens the hairpin structure, revealing the toehold t_r and the extended domain c . The $GATE\text{-Extract}$ is modified with a biotin group at the 5' end. By leveraging the strong affinity between streptavidin MBs and biotin, $GATE\text{-Extract}$ is anchored to the MB surface, thereby completing the extraction of the carried information.

An implementation of Ternary DNA Half-Adder and 1-trit Full Adder Using CB circuit. A ternary half-adder is designed to add two ternary digits, producing two outputs: a sum S_{out} and a carry C_{out} . This operation is performed without considering carry information. To calculate the sum of two inputs, $inputA_i$ and $inputB_j$, we utilize the ij -module. Let's examine the case where $i = 2$ and $j = 2$. Notably, other cases follow a similar method. In our implementation, $inputA_2$ and $inputB_2$ are introduced into the ij -module. These inputs interact with $GATE1_{22}$, resulting in the gradual displacement of the b_2 strand from $GATE1_{22}$. Since the 3' end of strand b_j is modified with a FAM fluorescent group, and the bottom strand of $GATE1_{22}$ is equipped with a BHQ1 quencher group, the FAM signal is triggered upon the displacement of strand b_2 . This results in an S_{out} value of 1, as illustrated in Figure 3c, curve 22. Concurrently, $inputA_2$ and $inputB_2$ in the test tube participate in a TMSD with $GATE_{ij}^-$ (Figure 4b), which displaces the strand $b_j r$. Subsequently, the strand $b_j r$ interacts with $GATE\text{-Convert}b_j$ to produce the carry C_{out} strand. In addition to the experiment described above, we also tested the other eight input combinations using ij -modules for $i, j \in \{0, 1, 2\}$, where $ij \neq 22$. The fluorescence output of each module matches the expected result (Figure 3c and Supporting Information, Figure S17), further validating the reliability of the ternary half-adder design.

We constructed a 1-trit full adder using our CB circuit. In comparison to the half-adder, the full adder includes an additional carry input, B_{in} , from the previous digit, making it a third input. This circuit also produces two outputs: a sum S_{out} and a carry

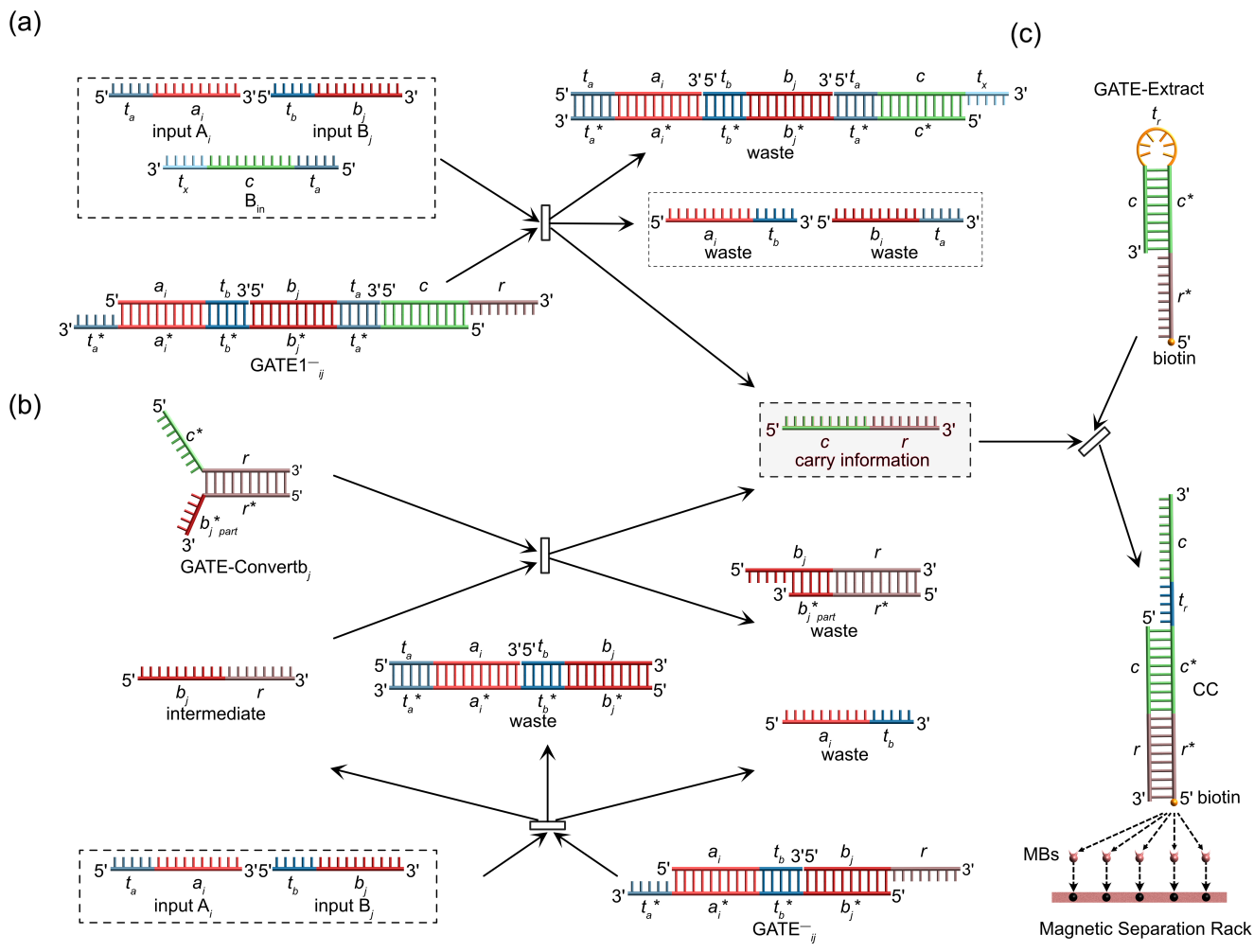


Figure 4. Generation and processing of carry information strands. (a) Schematic diagram of the three-input AND gate reaction for processing the first type of scenarios. (b) Schematic diagram of the two-input AND gate reaction for processing the second type of scenarios. (c) Extraction operation for the carry information strands.

C_{out} . We employed the ij -module to compute the addition of two addend inputs alongside the carry input B_{in} (serving as the blocking strand). For illustrative purposes, we set $i = 2$ and $j = 2$; other cases can be treated similarly. The implementation involves four logic gates: $GATE1_{22}$, $GATE2$, $GATE_{22}^-$, and $GATE-Convertb_2$. Specifically, the CB circuit allows B_{in} to block the toehold domain of $GATE1_{22}$ (Equation 2), preventing it from reacting with input A_2 and input B_2 . At the same time, B_{in} engages in strand displacement with $GATE2$ (Equation 3), resulting in the release of the strand c labeled with a VIC fluorophore at its 3' end. The detection of this VIC fluorescence signal indicates that $S_{out} = 2$. Concurrently, input A_2 and input B_2 undergo strand displacement with $GATE_{22}^-$ (Figure 4b), releasing the strand $b_2 r$, which then interacts with $GATE-Convertb_2$ to ultimately generate the carry C_{out} . Experimental results show that B_{in} effectively blocked $GATE1_{22}$, limiting the fluorescence intensity of the leakage reaction between input A_2 and input B_2 with $GATE1_{22}$ to below 0.5 (Figure 3e). This mechanism, which redirects the reaction to $GATE2$ and B_{in} , yielded VIC fluorescence output corresponding to the correct result 2 (Supporting Information, Figure S18). In addition to the aforementioned experiments, we also evaluated the other eight input combinations using ij -modules (where $i, j \in \{0, 1, 2\}$ and $ij \neq 22$). Each of these combinations successfully generated a fluorescence signal indicating the correct output (Figure 3d and Supporting Information, Figure S18). Furthermore, in contrast to the half-adder (where outputs were exclusively SUM1 result information), when B_{in} is present, all input combinations yielded SUM2 result information. Crucially, the corresponding SUM1 result information (generated by the leakage reaction) consistently remained below half of the SUM2 result information (Figure 3e). To further analyze the absolute output and absolute leakage for each input combination in the presence of B_{in} , we normalized all fluorescence signals (including both valid outputs and leakage)

to the highest fluorescence value. The experimental results show that the normalized SUM1 leakage signal intensity remains consistently below half of the SUM2 output signal intensity. (see Section S9 of the Supporting Information) This decisively demonstrates the effectiveness of the CB circuit in the adder.

The Implementation of Multi-digit Ternary DNA Full Adder Using CB Circuit. To effectively manage the propagation of carry information for each digit in a multi-trit adder, we utilized streptavidin MBs to extract and transfer carry information. Streptavidin is a protein known for its exceptional binding affinity to biotin^{59,60}. Since the carry information strand is not the B_{in} strand required for subsequent carry propagation, we designed an amplification-and-conversion reaction (Figure 5a). First, the GATE-amplifier transforms the Carry Carrier (CC) into B_{in} strands. Then, to compensate for signal loss inherent in TMSD and for losses during magnetic-bead extraction and transfer, we introduce fuel strands that further react with the intermediate strand generated from CC and GATE-amplifier, regenerating CC and thereby cyclically producing more B_{in} strands for downstream carry calculations. Experiments show that this amplification reaction increases B_{in} strand yield by approximately threefold (see Section S10 of the Supporting Information). The specific procedure is detailed below: The completed computational system is positioned on a magnetic rack, where GATE-Extract bound to streptavidin MBs is attracted to the bottom of the test tube via magnetism. After removing the supernatant (which contains unneeded waste), the GATE-amplifier and fuel strands are introduced. During experiments, it was observed that even in the absence of CC, a fluorescent signal was still produced. The reason this happened is that the GATE-amplifier, intended for signal amplification, can react similarly to B_{in} , though with lower efficiency. To mitigate this issue, we modified the 5' end of the single strand located below the GATE-amplifier with biotin. After signal amplification, we placed the reaction system on a magnetic rack again, thereby drawing the GATE-amplifier to the bottom of the test tube. Following this, the supernatant was collected as the B_{in} input for the next digit. This approach prevents misrecognition and ensures the accurate transfer of carry information.

To evaluate the feasibility of the multi-digit ternary full adder, we conducted an operational test using a ten-digit ternary full adder, focusing on the addition $1012212101 + 2211220122$. The procedure began by adding input A_1 and input B_2 to the designated test tube for the 12-module, followed by measurement of the resulting digit's fluorescent signal. Subsequently, carry information was extracted through magnetic selection and subjected to a signal amplification reaction. After another round of magnetic selection, the supernatant was transferred to the next digit calculation module along with the next digit's inputs (input A_0 and input B_2). The output from the fluorescent reporter gate was then recorded. This process continued until all digit calculations were complete (Figure 5b). Additionally, to enable an intuitive comparison of leakage rates at each digit, we predetermined the fluorescence intensity ratios among the three dyes through 15 independent experiments (see Section S11 of the Supporting Information) and uniformly normalized all subsequent data accordingly. The results are illustrated in Figure 5c, where the green, orange, and blue curves correspond to the fluorescence signals of ROX, FAM, and VIC, representing values of 0, 1, and 2, respectively. For each digit, the number indicated by the fluorescence species with the maximum fluorescence value (where all other fluorescence readings fall below half of this maximum) is deemed the final result for that digit. The overall result presented in the figure is 11001210000, thereby confirming both the feasibility and accuracy of the design.

To rigorously evaluate the scalability of the CB-circuit-based ternary adder, we adopted "consecutive carry capability" as the key metric. Should consecutive carries terminate, the B_{in} strand concentration is reset, and the true scalability is masked; hence, the upper limit of consecutive carries directly determines the scalability boundary. We thus designed a full consecutive-carry test: the adder achieves 100% success for up to eight consecutive carries, whereas success drops to 33.33% when consecutive carries reach the 9th and 10th digits (Figure 5d). Restricting our analysis to 100% successful cases, we conclude that the consecutive-carry capability of the CB ternary adder is eight digits.

Experimental Expansion of Digit Positions for the Multi-digit DNA Ternary Full Adder. Due to the inherent limitations of biochemical experiments, multi-digit DNA adders face a core challenge during actual operation: as the number of consecutive carry digits increases, the quantity of the carry information strand progressively diminishes, leading to computational errors. This is the fundamental reason impacting the scalability of DNA adders. Our design addresses this challenge by decoupling the computation of the result digit from that of the carry. The CA strategy allows us to enhance the performance by adjusting the concentration ratios of the relevant components. In particular, reducing the concentration of GATE 1_{ij} enables it to be more effectively bound by B_{in} (the carry generated from the previous digit), thereby minimizing signal leakage.

To validate this finding, we compared the experimental results from two different concentration configurations: 1) a GATE 1_{ij} concentration of 1 μ M and a GATE 1_{ij} concentration of 0.4 μ M; and 2) a GATE 1_{ij} concentration of 1 μ M and a GATE 1_{ij} concentration of 0.2 μ M. The results, illustrated in Figure 5d, indicate that with the higher concentration of GATE 1_{ij} in the first case, the carry information from the preceding digit must block more GATE 1_{ij} molecules, leading to a decrease in the amount of carry information available for carry calculation. Consequently, as the number of digits increases, the carry information exhibits a trend of accelerated attenuation, which in turn results in a significant reduction in the carry information contributing to the sum calculation. The fluorescence signal for the sum digit decays notably faster in this scenario compared to the second case. Note that even without the introduction of the CA strategy, we could still achieve eight consecutive carry calculations (Figure 5d). This is because our judgment was based on the maximum fluorescence value for each digit, requiring other fluorescence

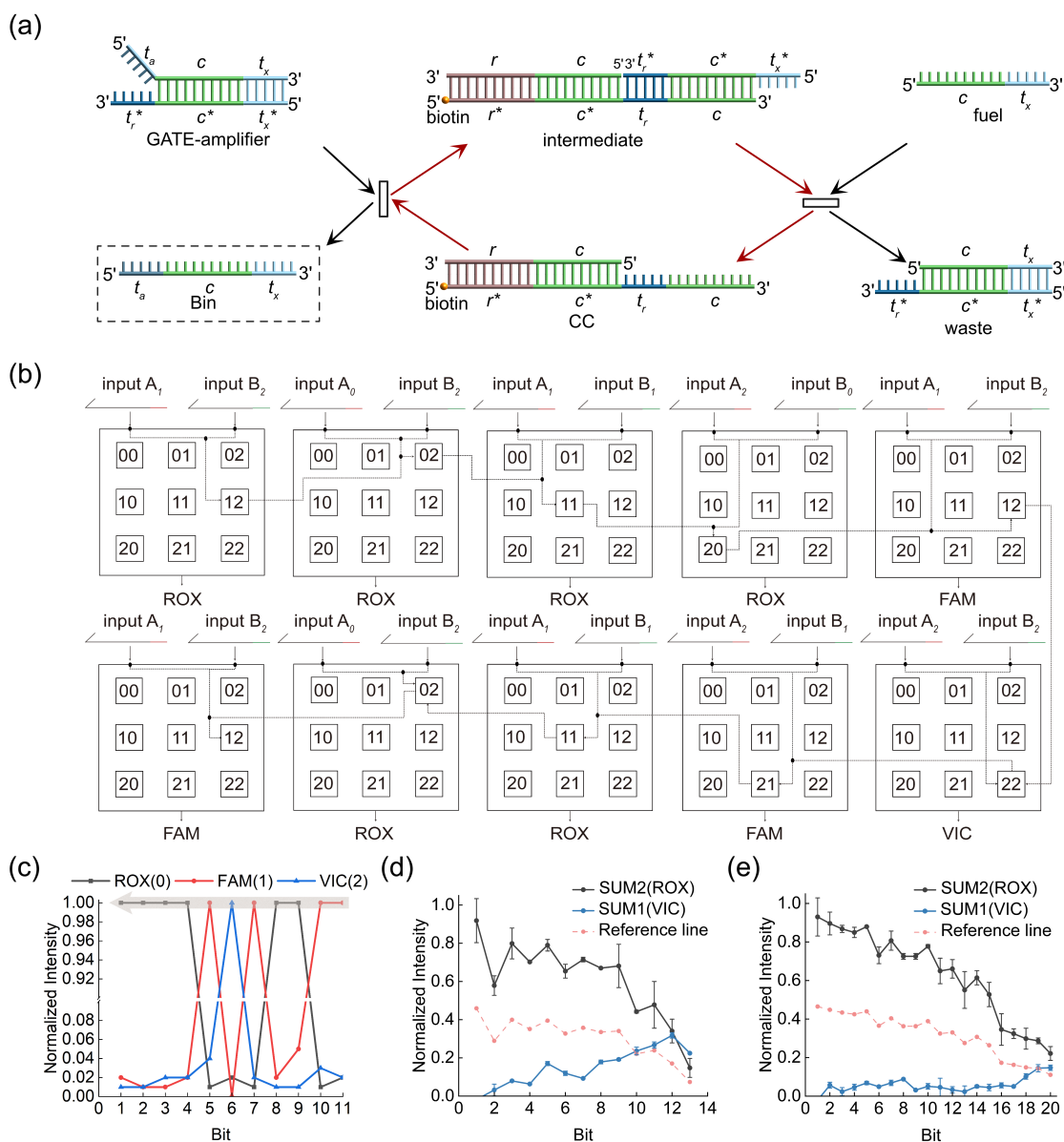


Figure 5. (a) Schematic diagram of the catalytic reaction for the carry information strand. (b) Reaction network of a multi-trit full adder calculating $1012122101 + 2210221122$. (c) The sum of two ten-digit ternary numbers. The final sum is read from the high digit to the low digit. (d) Computational performance of the ternary adder under continuous-carry conditions without the CA strategy, illustrated with the example $102102102101 + 120120120122$, where the reference line represents half of the SUM2 signal, i.e., the leakage threshold. (e) Computational performance of the ternary adder under continuous carry conditions with the CA strategy, illustrated with the example: $2102102102102101 + 0120120120120122$, where the reference line represents half of the SUM2 signal, i.e., the leakage threshold.

values to be less than half that maximum. Therefore, even as the information continuously decayed, the leakage rate (i.e., the ratio of the maximum fluorescence value corresponding to non-maximal fluorescence types to the maximum fluorescence value) remained below 0.5, allowing us to perform consecutive multi-digit carry calculations. Based on this, we further evaluated changes in the leakage rate as the number of digits increased following the introduction of the CA strategy. The results show that the leakage rate was significantly reduced after the introduction of the CA strategy (Figure 5d and Figure 5e). Additionally, the CA strategy helps to reduce signal attenuation. In particular, as the digit count increases, the adder employing the CA strategy demonstrates a slower decay rate in the fluorescence signal that indicates the correct result (see Figure 5d) compared to the adder that does not utilize the CA strategy (see Figure 5e). This strongly demonstrates the effectiveness of our proposed CA strategy.

To assess the practical upper limit of the CA strategy, we performed a 17-consecutive-carry ternary addition and successfully

obtained the correct output. However, the 18th carry failed because the leakage rate exceeded the detection threshold, thereby establishing the current system's maximum reliable depth at 17 carries (see Figure 5e). Additionally, we examine in detail the applicability of the CA strategy in Section S13 of the Supporting Information. This achievement represents a significant advancement over the current state-of-the-art multi-bit adder based on DNA circuits, which has only achieved four consecutive carries. In terms of computational scale, our result is 8.61×10^6 times that of the recently reported study (detailed calculations are provided in Supporting Information s1.2); compared to an advanced binary adder implemented using non-DNA circuit technology (which achieves 25 consecutive carries), our result is 3.85 times its computational scale. Furthermore, given differences in the number of strands used across adders, we introduced the "scale/strand" metric to more reasonably evaluate the computational capability of the adders. Under this metric, our achievement reaches 2.41×10^6 times and 30.6 times that of the two aforementioned comparison targets, respectively. Additionally, we analyzed the per-digit leakage of our adder, all of which remained within acceptable ranges (detailed calculations are provided in Supporting Information s1.1). Furthermore, our adder achieves the best performance in terms of the number of strands per digit (detailed calculations are provided in Supporting Information s1.2). This finding provides a promising direction for future design optimization of higher-digit full adders.

To intuitively illustrate the scalability advantage of the higher radix, we first developed 9-digit binary and 8-digit ternary full adders (both featuring consecutive carries) within the same CB-circuit core architecture. As depicted in Figure 5d and Figure S24, both types operate with a comparable digit count, yet the computational capability of the binary adder is only about 7.79% that of the ternary adder (refer to Supporting Information S12 for further details). Additionally, using the CA strategy, we constructed 17-digit binary and 17-digit ternary full adders (with consecutive carries). The experimental outcomes presented in Figure 5e and Figure S25 demonstrate that both adders once again maintain the same digit count; however, the computational scale of the binary adder is a mere 0.1% of that of the ternary adder (see Supporting Information S12 for more details). These two adders achieve comparable digit depths, as the per-digit signal attenuation is similarly aligned under the identical CB/CA core architecture (as illustrated in Figures S26 and S27). Thus, within the same framework, the ternary implementation clearly offers a significant advantage.

CONCLUSIONS

This paper reports the first experimental realization of a DNA-based ternary full adder. To achieve this, we designed a chemically kinetic logic control circuit (CB circuit) that cleverly exploits differences in reaction rate constants to enable dynamic selection and blocking of reaction pathways. Second, by applying the principles of chemical equilibrium, we propose a CA strategy based on a divide-and-conquer approach. This strategy empowers the circuit to regulate reactant concentration ratios, thereby optimizing signal transmission efficiency. Subsequently, these two innovations have led to the successful realization of a ternary DNA full adder. This innovative ternary DNA adder significantly overcomes the computational scale limitations of traditional DNA adders. Experimental results demonstrate that the maximum computational scale achievable by the DNA adder with consecutive carries is improved by approximately 8.61×10^6 times compared to existing DNA circuit-based four-consecutive-carry adders. Meanwhile, it also achieves a 3.85-fold improvement in computational scale over advanced binary adders implemented using thermodynamic methods, representing a significant enhancement. Moreover, our adder also performs favorably across various other evaluation metrics (e.g., scale per strand, strands per digit; see Supporting Information, Section S1 for detailed comparisons). While achieving infinite carry propagation remains a challenge, the experimental findings fully demonstrate the validity and efficiency of our approach.

Although we have not yet directly characterized addition circuits beyond seventeen consecutive carries, several strategies can further extend scalability: (i) introducing additional leakage-filter modules or lower-leakage strand-displacement schemes (e.g., using clamps in the seesaw circuits); (ii) fine-tuning the CA strategy to further strengthen the carry-information strand; (iii) circuit optimization, such as employing enzymes to achieve more efficient strand displacement and thus reduce signal attenuation; and (iv) spatial localization, anchoring computational modules at distinct locations (e.g., specific sites on DNA origami or on separate magnetic beads/nanoparticle surfaces) to prevent signal molecules from diffusing throughout the bulk solution, minimize crosstalk, and ensure that signals are delivered to neighboring modules along predefined paths. Collectively, these approaches provide a clear roadmap for pushing the DNA ternary-adder architecture beyond the current experimentally demonstrated number of carry digits.

The realization of a ternary DNA full adder represents a significant advancement in biomolecular computing. Our research not only enhances computational capabilities but also helps reduce costs, making DNA computing more practical and sustainable. Additionally, the CB circuit can process multiple input signals based on their priority, providing a powerful tool for developing more complex DNA computing systems. This also highlights the immense potential of DNA computing in advancing the chemistry of molecular information processing. Moreover, the CA strategy and the module partitioning method provide a new perspective for reducing the impact of leakage reactions on circuit performance. More importantly, the successful application of the CB circuit and CA strategy provides new insights and tools for designing and constructing more complex and robust chemical reaction-based molecular systems, extending beyond computation into areas such as sensing, diagnostics, and

drug-delivery control.

To develop a more intelligent, automated ternary multi-digit full adder, we aim to integrate microfluidic technology with other techniques. This integration will enable the immobilization of magnetic beads within microchannels and achieve fully automated, continuous addition operations through programmed valve-based flow switching. The ternary full adder has the potential to optimize the performance of complex systems and may offer unique advantages in areas such as artificial intelligence, neural networks, and cryptography in the future.

Methods

Materials. DNA oligonucleotides were purchased from Sangon Biotech (Shanghai) Co., Ltd. and purified by high-performance liquid chromatography (HPLC). All DNA strand sequences used in biochemical experiments were initially designed using NUPACK and subsequently manually optimized to ensure GC content remained between 30% and 60%. The full list of sequences used in this study is provided in Table 3 of Section S14 in the Supporting Information. Unmodified DNA strands were dissolved in 1× TE buffer and stored at −20°C. Fluorescently labeled or quencher-modified strands were dissolved in deionized water and stored at −20°C in the dark. DNA concentrations were measured using a NanoPhotometer N120. Prior to experiments, DNA samples were prepared by mixing with 12.5 mM $MgCl_2$ in 1× TE buffer.

The DNA complexes were assembled by mixing equimolar amounts of the corresponding single-stranded DNA oligonucleotides and then annealing in a PCR thermocycler. The annealing protocol consisted of an initial denaturation at 95°C for 2 min, followed by a gradual cooling: from 95°C to 65°C at a rate of 0.1°C every 3s, then to 35°C at 0.1°C every 6s, and finally to 4°C at 0.1°C every 3s. The annealed complexes were stored at 4°C for subsequent use. For fluorescently labeled or quencher-modified complexes, the cooling rate after the initial denaturation (95°C, 2 min) was set to 0.1°C every 6s down to 4°C, after which the samples were stored at 4°C until use.

Fluorescence Kinetics Experiments. In fluorescence-kinetics assays, the target DNA concentration was inferred from the measured fluorescence intensity. DNA samples were prepared according to the experimental design, with 1× defined as 1 μM. Final concentrations corresponded to 2× input gate and 1× reaction gate. Fluorescence was monitored using a QuantStudio 3&5 Real-Time PCR System (Thermo Fisher Scientific, Waltham, MA, USA) equipped with a 96-well fluorescence plate reader. The thermal profile was set as follows: during the holding stage, the temperature was decreased to 1.6°C at 4°C/s and held for 10s before the PCR stage; subsequently, the temperature was ramped up to 23°C at 3°C/s, and fluorescence readings were acquired every 10s. All fluorescence curves were normalized to allow for direct comparison across experiments.

Statistical Analysis. Normalization method: Fluorescence correction was performed via 15 independent experiments—under identical circuit and sequence conditions, single-dye reactions (ROX, FAM or VIC) were run in full, the intensity of each dye was recorded in all three channels, and the brightest ROX was set as reference (1.00) to yield the correction ratio ROX:FAM:VIC = 1.00:0.939:0.261; all subsequent readings were corrected by these factors. Normalization formula: $x_{\text{norm}} = (x - x_{\text{min}})/(x_{\text{max}} - x_{\text{min}})$. Data presentation: Results are shown as mean ± SD; consecutive-carry experiments used two replicates, whereas data from the half-adder and one-digit full adder are plotted using a single dataset; all remaining experiments used three replicates. Statistical analyses were performed using OriginPro 2024.

References

1. Goñi-Moreno, A. & Nikel, P. I. High-performance biocomputing in synthetic biology—integrated transcriptional and metabolic circuits. *Frontiers in bioengineering and biotechnology* **7**, 40 (2019).
2. Adleman, L. M. Molecular computation of solutions to combinatorial problems. *science* **266**, 1021–1024 (1994).
3. Fan, D., Wang, J., Wang, E. & Dong, S. Propelling dna computing with materials' power: recent advancements in innovative dna logic computing systems and smart bio-applications. *Advanced Science* **7**, 2001766 (2020).
4. Kim, S. & Gang, J. The detection of a mismatched dna by using hairpin dna-templated silver nanoclusters. *Analytical Biochemistry* **549**, 171–173 (2018).
5. Gasser, S. *et al.* Sensing of dangerous dna. *Mechanisms of ageing and development* **165**, 33–46 (2017).
6. Spencer, D. M., Reyna, A. G. & Pisetsky, D. S. The binding of monoclonal and polyclonal anti-z-dna antibodies to dna of various species origin. *International Journal of Molecular Sciences* **22**, 8931 (2021).
7. Jingjing, M. Three-input logic gate based on dna strand displacement reaction. *Scientific Reports* **13**, 15210 (2023).
8. Zhou, C., Liu, D., Wu, C., Dong, S. & Wang, E. Multifunctional graphene/dna-based platform for the construction of enzyme-free ternary logic gates. *ACS Applied Materials & Interfaces* **8**, 30287–30293 (2016).
9. Zhang, C., Paluzzi, V. E., Sha, R., Jonoska, N. & Mao, C. Implementing logic gates by dna crystal engineering. *Advanced Materials* **35**, 2302345 (2023).

10. Allemani, C. *et al.* Global surveillance of trends in cancer survival 2000–14 (concord-3): analysis of individual records for 37 513 025 patients diagnosed with one of 18 cancers from 322 population-based registries in 71 countries. *The Lancet* **391**, 1023–1075 (2018).
11. Zandvakili, I. & Lazaridis, K. N. Cell-free dna testing: future applications in gastroenterology and hepatology. *Therapeutic Advances in Gastroenterology* **12**, 1756284819841896 (2019).
12. Shieh, P. B. Advances in the genetic testing of neuromuscular diseases. *Neurologic Clinics* **38**, 519–528 (2020).
13. Yang, Q. *et al.* Dna logic circuits for multiple tumor cells identification using intracellular microrna molecular bispecific recognition. *Advanced healthcare materials* **10**, 2101130 (2021).
14. Chen, C., Wen, J., Wen, Z., Song, S. & Shi, X. Dna strand displacement based computational systems and their applications. *Frontiers in Genetics* **14**, 1120791 (2023).
15. Xu, J., Chen, C. & Shi, X. Graph computation using algorithmic self-assembly of dna molecules. *ACS Synthetic Biology* **11**, 2456–2463 (2022).
16. Liu, L., Li, Y., Wang, Y., Zheng, J. & Mao, C. Regulating dna self-assembly by dna–surface interactions. *ChemBioChem* **18**, 2404–2407 (2017).
17. Oishi, M. Comparative study of dna circuit system-based proportional and exponential amplification strategies for enzyme-free and rapid detection of mirna at room temperature. *ACS omega* **3**, 3321–3329 (2018).
18. Lv, H., Li, Q., Shi, J., Fan, C. & Wang, F. Biocomputing based on dna strand displacement reactions. *ChemPhysChem* **22**, 1151–1166 (2021).
19. Wang, B., Wang, S. S., Chalk, C., Ellington, A. D. & Soloveichik, D. Parallel molecular computation on digital data stored in dna. *Proceedings of the National Academy of Sciences* **120**, e2217330120 (2023).
20. Seelig, G., Soloveichik, D., Zhang, D. Y. & Winfree, E. Enzyme-free nucleic acid logic circuits. *science* **314**, 1585–1588 (2006).
21. Elbaz, J. *et al.* Dna computing circuits using libraries of dnazyme subunits. *Nature nanotechnology* **5**, 417–422 (2010).
22. Orbach, R. *et al.* A full-adder based on reconfigurable dna-hairpin inputs and dnazyme computing modules. *Chemical Science* **5**, 3381–3387 (2014).
23. Liu, C. *et al.* Cross-inhibitor: a time-sensitive molecular circuit based on dna strand displacement. *Nucleic acids research* **48**, 10691–10701 (2020).
24. Lv, H. *et al.* Dna-based programmable gate arrays for general-purpose dna computing. *Nature* **622**, 292–300 (2023).
25. Wang, F. *et al.* Implementing digital computing with dna-based switching circuits. *Nature communications* **11**, 121 (2020).
26. Weng, Z. *et al.* Cooperative branch migration: a mechanism for flexible control of dna strand displacement. *ACS nano* **16**, 3135–3144 (2022).
27. Wu, L., Wang, G. A. & Li, F. Plug-and-play module for reversible and continuous control of dna strand displacement kinetics. *Journal of the American Chemical Society* **146**, 6516–6521 (2024).
28. Qian, L. & Winfree, E. Scaling up digital circuit computation with dna strand displacement cascades. *science* **332**, 1196–1201 (2011).
29. Qian, L., Winfree, E. & Bruck, J. Neural network computation with dna strand displacement cascades. *nature* **475**, 368–372 (2011).
30. Evans, C. G. & Winfree, E. Physical principles for dna tile self-assembly. *Chemical Society Reviews* **46**, 3808–3829 (2017).
31. Woods, D. *et al.* Diverse and robust molecular algorithms using reprogrammable dna self-assembly. *Nature* **567**, 366–372 (2019).
32. Sarraf, N., Rodriguez, K. R. & Qian, L. Modular reconfiguration of dna origami assemblies using tile displacement. *Science Robotics* **8**, eadf1511 (2023).
33. Amir, Y. *et al.* Universal computing by dna origami robots in a living animal. *Nature nanotechnology* **9**, 353–357 (2014).
34. Chatterjee, G., Dalchau, N., Muscat, R. A., Phillips, A. & Seelig, G. A spatially localized architecture for fast and modular dna computing. *Nature nanotechnology* **12**, 920–927 (2017).
35. Bui, H. *et al.* Localized dna hybridization chain reactions on dna origami. *ACS nano* **12**, 1146–1155 (2018).

36. Li, Z. *et al.* Programming directional strand polymerization on dna origami for logic computing. *Small Structures* 2500220 (2025).
37. Song, T. *et al.* Improving the performance of dna strand displacement circuits by shadow cancellation. *ACS nano* **12**, 11689–11697 (2018).
38. Turberfield, A. J. *et al.* Dna fuel for free-running nanomachines. *Physical review letters* **90**, 118102 (2003).
39. Zhang, D. Y., Turberfield, A. J., Yurke, B. & Winfree, E. Engineering entropy-driven reactions and networks catalyzed by dna. *Science* **318**, 1121–1125 (2007).
40. Zhang, D. Y. & Winfree, E. Control of dna strand displacement kinetics using toehold exchange. *Journal of the American Chemical Society* **131**, 17303–17314 (2009).
41. Mehra, V. C. R. 2-bit comparator using different logic style of full adder. *Int. J. Soft Comput. Eng. IJSCE* **3**, 277–9 (2013).
42. Imana, J. L. Fast bit-parallel binary multipliers based on type-i pentanomials. *IEEE Transactions on Computers* **67**, 898–904 (2017).
43. Navi, K., Moaiyeri, M. H., Mirzaee, R. F., Hashemipour, O. & Nezhad, B. M. Two new low-power full adders based on majority-not gates. *Microelectronics journal* **40**, 126–130 (2009).
44. Kouretas, I., Basetas, C. & Paliouras, V. Low-power logarithmic number system addition/subtraction and their impact on digital filters. *IEEE Transactions on Computers* **62**, 2196–2209 (2012).
45. Aguirre-Hernandez, M. & Linares-Aranda, M. Cmos full-adders for energy-efficient arithmetic applications. *IEEE transactions on very large scale integration (VLSI) systems* **19**, 718–721 (2010).
46. Tang, Z., Li, S., Chen, C., Zhou, Z. & Yin, Z. A localized scalable dna logic circuit system based on the dna origami surface. *International Journal of Molecular Sciences* **26**, 2043 (2025).
47. Li, H. *et al.* Implementation of arithmetic functions on a simple and universal molecular beacon platform. *Advanced Science* **2**, 1500054 (2015).
48. Han, W. & Zhou, C. 8-bit adder and subtractor with domain label based on dna strand displacement. *Molecules* **23**, 2989 (2018).
49. Park, K. S., Seo, M. W., Jung, C., Lee, J. Y. & Park, H. G. Simple and universal platform for logic gate operations based on molecular beacon probes. *Small* **8**, 2203–2212 (2012).
50. Li, W., Zhang, F., Yan, H. & Liu, Y. Dna based arithmetic function: a half adder based on dna strand displacement. *Nanoscale* **8**, 3775–3784 (2016).
51. Su, H., Xu, J., Wang, Q., Wang, F. & Zhou, X. High-efficiency and integrable dna arithmetic and logic system based on strand displacement synthesis. *Nature communications* **10**, 5390 (2019).
52. Huang, D. *et al.* Versatile and homogeneous dna tetraplex platform for constructing label-free logic devices: From design to application. *Chemistry—A European Journal* **25**, 6996–7003 (2019).
53. Tandon, A. *et al.* Demonstration of arithmetic calculations by dna tile-based algorithmic self-assembly. *ACS nano* **14**, 5260–5267 (2020).
54. Xie, N. *et al.* Scaling up multi-bit dna full adder circuits with minimal strand displacement reactions. *Journal of the American Chemical Society* **144**, 9479–9488 (2022).
55. Stérin, T., Eshra, A., Adio, J., Evans, C. G. & Woods, D. A thermodynamically favoured molecular computer: Robust, fast, renewable, scalable. *bioRxiv* 2025–07 (2025).
56. Hayes, B. Third base. *American scientist* **89**, 490–494 (2001).
57. Jeong, J. W. *et al.* Tunnelling-based ternary metal–oxide–semiconductor technology. *Nature Electronics* **2**, 307–312 (2019).
58. Xu, J., Liu, W., Zhang, K. & Zhu, E. Dna coding theory and algorithms. *Artificial Intelligence Review* **58**, 178 (2025).
59. Ozawa, M., Ozawa, T., Nishio, M. & Ueda, K. The role of ch/π interactions in the high affinity binding of streptavidin and biotin. *Journal of Molecular Graphics and Modelling* **75**, 117–124 (2017).
60. Zhang, S., Wang, K., Huang, C. & Sun, T. Reconfigurable and resettable arithmetic logic units based on magnetic beads and dna. *Nanoscale* **7**, 20749–20756 (2015).

Acknowledgements

This work was supported by the National Major Scientific Instrument and Equipment Development Project of the National Natural Science Foundation of China (No. 62427811) and the National Natural Science Foundation of China (No. 62272115). The authors declare no competing financial interest.

Author contributions

Conceptualization, E.Z. and P.Q.; Investigation, E.Z., X.L. and C.L.; Methodology, J.X., X.L. and P.Q.; Supervision, X.L. and C.L.; Writing-original draft, E.Z, P.Q. and X.L.; Writing-review and editing, E.Z. and C.L. All authors have read and agreed to the published version of the manuscript.